Solar-Terrestrial Physics. 2026, vol. 12, iss. 2, pp. 76–88. DOI: 10.12737/stp-122202609. © 2026 O.I. Berngardt Published by INFRA-M Academic Publishing House

DOI: 10.12737/stp-122202609
EDN: NRJATV

Received July 18, 2025
Accepted January 23, 2026

METHOD FOR ESTIMATING PARAMETERS OF MULTI-MODE SIGNALS MEASURED AT SECIRA RADARS

O.I. Berngardt
Institute of Solar-Terrestrial Physics SB RAS,
Irkutsk, Russia, berng@iszf.irk.ru

Abstract. The paper presents the algorithm for evaluating parameters of coherent scattering signals, which is based on the assessment of their parametric spectra by the well-known autoregression ARMA(10,10) model. The assessment consists of autoregression over 10 sequence members, moving average over residuals for 10 sequence members, and subsequent fitting of the resulting spectra with the sum of gaussian functions. The algorithm is a development of Burg's method, previously proposed for the analysis of SuperDARN data. It differs from the method in the use of a more complex regression model, consideration of characteristics of the correlation function, and determination of three parameters for each peak (mode) — amplitude, Doppler velocity, and spectral width. Comparison shows that the best continuity between the parameters of multi-mode signals, obtained by new and standard signal processing methods, is provided by analysis of the mode with maximum integral power. The analysis has revealed that new and standard methods in the case of single-mode signals give close Doppler velocities. The multi-mode analysis presented in the paper increases the number of detected signals of various types, and can be employed to expand the diagnostic capabilities of SECIRA/SuperDARN radars, including automatic classification of each mode.

Keywords: decameter radar, SECIRA, ionosphere, multi-mode signals.

INTRODUCTION

Coherent scatter radars of SuperDARN [Greenwald et al., 1995; Chisham et al., 2007; Nishitani et al., 2019], CN-DARN [Zhang, 2024], and SECIRA [Berngardt et al., 2022] networks use scattered signals to analyze processes in ionospheric plasma: from large-scale (based on data from scattering from Earth's surface) to small-scale (based on data from scattering by ionospheric irregularities) irregularities in the mid- and high-latitude ionosphere. In this case, processing of data used for analysis is usually divided into three stages:

- recording of quadrature components of scattered signal (IQ);
- the subsequent construction of averaged autocorrelation functions of received signal (ACFs) from measurements with the main phased antenna array of the radar and the cross-correlation function (CCF) between measurements with the main and interference phased antenna arrays of the radar;
- final processing of ACF (FITACF) to obtain interpretable geophysical parameters from them. The scattered signal power provides information on the irregularity scattering cross-section, signal amplification/attenuation due to radio wave focusing in the inhomogeneous ionosphere, aspect sensitivity of scattering irregularities, as well as radio wave absorption along the propagation path. The Doppler frequency shift and spectral signal broadening allow us to estimate line-of-sight velocities of irregularities and their lifetime respectively. The final processing of CCF makes it possible to determine the elevation angle of scattered radio wave arrival.

Received signals are usually interpreted after processing signal autocorrelation functions (hereinafter CF) by the FITACF algorithm [Ribeiro et al., 2013], which derives the Doppler signal shift from CF — the velocity V_d and CF form parameters in two models of exponential CF decay with time: linear/exponential (l) and squared/Gaussian (s). As a result, the processed data usually consists of five main parameters: signal power in the two models (P_l, P_s), spectral signal width in units of velocity in the two models (W_l, W_s), and the Doppler velocity of irregularities along the line of sight V_d. The FITACF algorithm is fundamental to further interpretation of data, is constantly upgraded, becomes more complex [Ribeiro et al., 2013; Ponomarenko et al., 2025], and is verified experimentally many times [Koustov et al., 1997, 2009, 2019, 2020; Xu et al., 2008; Bahcivan et al., 2013; Ponomarenko et al., 2025].

One well-known example that prevents effective processing of received signals by the FITACF method is the observation of multi-mode signals [Schiffler et al., 1997; Huber, Sofko, 2000; Shepherd et al., 2003; Danskin et al., 2004; Koustov et al., 2005] — signals that have several spectral peaks and do not fit the FITACF model. Various methods can be employed to process such signals, which are based on spectral estimation of a signal by the Fourier transform [Nguyen et al., 2014], the MUSIC method [Barthes et al., 1998], or Burg's parametric spectral estimation method [Schiffler et al., 1997]. Obviously, the automatic method for processing coherent radar signals, which adapts to experimental observations, must take into account the existence of multi-mode signals, and be capable of identifying parameters of each mode.

Thus, the five-parameter model underlying FITACF does not seem to have the necessary complexity to fully describe experimental data. The presence of the two independent models (exponential and Gaussian) for describing CF implies that they can be arbitrarily selected and hence arbitrarily interpreted by a researcher; therefore, at least one additional parameter responsible for choosing an adequate model is required.

To eliminate such arbitrariness, a new multiparametric method for processing CF of received signals from coherent scatter radars is proposed, which expands the capabilities of the FITACF algorithm and is an improvement on Burg's method put forward in [Schiffler et al., 1997].

PARAMETRIC SPECTRAL MODEL OF A SIGNAL

Signal correlation function form

Figure 1, *a–d* exemplifies signal CF forms. CF measured by radars is obtained only for nonnegative delays, and Figure 1 shows its full form, symmetrically (complex conjugate) extended to the left. This extension is related to the mathematical formulation of the problem and the ergodic hypothesis, which reduces averaging over sounding runs to ensemble averaging. Note that CF at the zero point in a multipulse sequence includes the energy of broadband noise at the receiver input. Therefore, CF at this point differs in amplitude from that at the remaining delays (see panels *c*, *d*), contains significant errors, and should either be ignored in the analysis or corrected before processing.

Thus, the CF the model should approximate can be determined in two ways: by neglecting the zero delay or by approximating it.

The first way (half CF) is to find the model from one part of signal ACF measured by the radar $R(\tau)$ (it does not matter whether it is left or right) without regard to zero delay. In this case, we use the left part (complex conjugate of the measured one):

$$R_{\text{model}}(\tau) = \begin{cases} 0, \tau \geq 0 \\ R^*(-\tau), \tau < 0 \end{cases} \quad (1)$$

The second way (zero-delay completion and interpolation) is to use a symmetrically completed with respect to CF with approximated CF at zero delay:

$$R_{\text{model}}(\tau) = \begin{cases} R(\tau), \tau > 0 \\ |R(\Delta\tau)|, \tau = 0 \\ R^*(-\tau), \tau < 0 \end{cases} \quad (2)$$

It is obvious from the formula that this CF value at zero delay corresponds to the linear approximation of the amplitude and phase at the zero point in adjacent values.

Panels *a–d* exemplify signal CF (two-sided, completed based on complex conjugate): the real (black line) and imaginary (orange line) parts. Panels *c* and *d* show a peculiarity of CF zero delay associated with the presence of broadband noise in the signal. The left part, complex conjugate of the right one, is indicated in panels *a–d* by solid lines; original radar observations, by dash-dot lines.

Parametric spectral estimate

The Wiener—Khinchin theorem suggests that any processing technique formulated for signal CF can also be described in terms of processing its spectral power. The parameters used by FITACF imply that the spectral representation is often more advantageous, since it is natural for

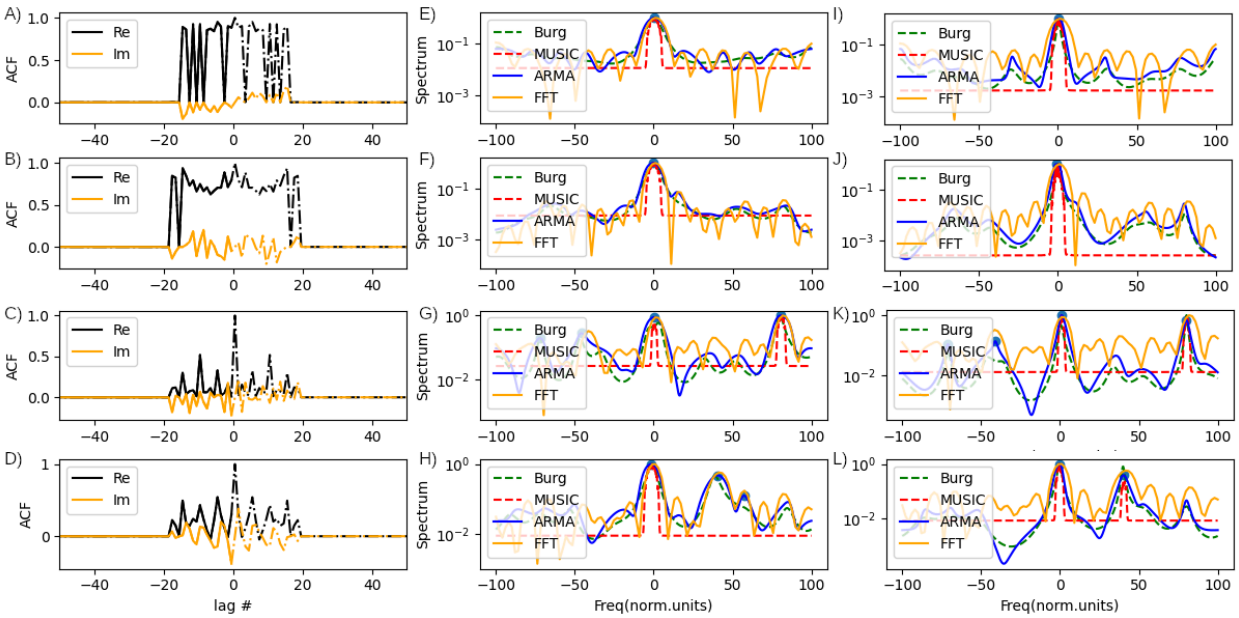

Figure 1. Examples of CFs (*a–d*), their spectral estimates from half CF (*e–h*) and full CF with interpolated zero delay (*i–l*). The spectral estimates were made using FFT, parametric spectral estimates by the Burg algorithm (AR model of order of 8), the ARMA model (of order of 10, 10), and the MUSIC model of order of 10 from EKB radar data for May 29, 2025. The dash-dot line (*a–d*) denotes radar measurement data; the solid line, data completed with complex conjugate

these parameters. The parameters derived from CF have a clear spectral interpretation: the power is the integral under the spectral power curve, the Doppler signal shift is the maximum probable or average frequency in the spectral signal power, the spectral width is spectral peak width.

The main disadvantages of spectral processing are the extremely small number of CF values (for a standard 7-pulse sounding signal, it is usually less than 20) and the so-called bad lags — points at which signal CF cannot be measured due to sounding signal characteristics. Therefore, standard spectral estimates often present difficulties. There are, however, more complex parametric spectral estimates, such as those proposed in [Schiffler et al., 1997; Barthes et al., 1998], which allow us to determine spectral characteristics of a signal from a relatively small number of points.

In panels *e–h* are Fourier spectra of CF (orange line) according to the Wiener—Khinchin theorem related to the received signal spectrum. The spectral power is seen to have often many peaks, especially for ionospheric signals. Most of the peaks are either noise interference or really nonexistent aliases associated with finiteness of the domain, where measured CF is not zero. This, in turn, is due to the finiteness of the sounding sequence that ranges from 7 to 16 pulses (from 60 to 250 ms) [Berngardt et al., 2020]. Finiteness of the sounding sequence makes it impossible to measure CF over the entire lifetime range of irregularities and to determine the number of real peaks in the spectrum. Traditionally, aliases are reduced by selecting a time window for spectral processing (Blackman, Kaiser, and other windows), but they additionally broaden the peaks in spectra and are therefore ineffective in the problem of separating close peaks, which arises in radars [Schiffler et al., 1997; Huber, Sofko, 2000; Shepherd et al., 2003; Danskin et al., 2004; Koustov et al., 2005].

To estimate the number of peaks in the spectrum, we use the parametric estimate of the spectrum by the autoregressive model ARMA [Cadzow, 1982], which builds a series model based on autoregression of values (AR part of the model) and moving averages of noise-like residuals (MA part of the model). Knowing coefficients of this model, we can construct a parametric spectral estimate of CF [Cadzow, 1982]. This model is an improvement on the Burg spectral estimate, which is based only on the AR model.

Estimation by half the correlation function

Panels *e–h* present the results of CF signal processing by four methods: Fourier transform, MUSIC, Burg, and ARMA parametric estimates. All the methods are applied to the left side of CF.

Panels *e–h* exhibit the classical Fourier spectrum (solid orange line) of CF (spectral power) and the parametric spectrum ARMA (10, 10) (solid blue line), constructed from this CF with numbers of coefficients of autoregression (AR) and moving average (MA) 10 and 10 respectively. The choice of such a number of regression coefficients is associated with a significant number of points in measured CF, which does not exceed 20. It can be seen that the parametric spectrum is smoother than the Fourier spectrum and contains fewer maxima (aliases). Circles denote all automatically determined local maxima whose amplitudes do not exceed 0.1 of the amplitude of the main (maximum) peak; green and red dashed lines are respectively the results of processing by the Burg algorithm for eight signal modes put forward in [Schiffler et al., 1997] and the 10-mode MUSIC method proposed in [Barthes et al., 1998]. Note that in [Danskin et al., 2004], the –8 dB threshold is utilized as a threshold for cutting off weak peaks for the Burg algorithm, which is close to the 0.1 threshold we employ.

The Burg algorithm is seen to describe the signal spectrum less accurately than ARMA, ignoring some peaks, especially in multi-mode signals, which is due to the random nature of scattering and random errors in determining CFs, which are not defined by the AR model, but are taken into account by the ARMA model.

It is also apparent that all the methods determine the main spectral peak in approximately the same way, differences are observed in the position of additional peaks and in the width of parametric spectra: the Burg estimate makes them narrower. The ARMA estimate make them broader, but more accurately describing the spectral width. Comparison of Figures shows that the MUSIC method is subjectively less accurate than the Burg or ARMA algorithms: it detects fewer peaks and the peaks themselves have an irregular structure near the maximum.

It can also be seen that the number of peaks is small and is expected to not exceed 10, which is related, among other things, to the number of regression coefficients.

Estimate based on the full correlation function with interpolated zero point

Figure 1 (*i–l*) presents the results of processing of similar signal CFs for full CF (left and right parts) with the interpolated zero point. It is obvious that all the methods determine the main spectral peak in approximately the same way; differences are observed in the position of additional peaks and in their amplitudes. The amplitudes and spectral widths of both estimates can be in arbitrary relation, but the Burg estimate is likely to give narrower ones than the ARMA estimate, which may be due to the lower order of the Burg model and its greater simplicity.

The MUSIC method is seen to be subjectively less accurate than the Burg or ARMA algorithms — despite it yielding the narrowest peaks, it reduces their detected number.

The quality of determining the position of peaks in a signal by the Burg and ARMA algorithms was compared statistically: each CF was evaluated by the Burg and ARMA methods, for which the minimum number of maxima in parametric spectra, whose amplitude exceeds half the amplitude of the main component, was found. Then, pairwise comparison between sums of amplitudes of Fourier spectra $P_{i,\mathrm{burg}}$ and $P_{i,\mathrm{arma}}$ was carried out at the frequencies obtained by the Burg and ARMA methods for each mode of each spectrum respectively:

$$N = \min\left(N_{\text{burg}}, N_{\text{arma}}\right),$$
$$P_{i,\text{arma}} = S\left(M_{i,\text{arma}}\right), \quad (3)$$
$$P_{i,\text{burg}} = S\left(M_{i,\text{burg}}\right).$$

Here, N_{burg}, N_{arma} are mode numbers determined by the Burg and ARMA algorithms; $M_{i,\text{burg}}$, $M_{i,\text{arma}}$ are positions of maxima found by these algorithms; S is the Fourier spectrum of ACF (spectral power).

The higher P, the closer the peaks, identified by such a parametric spectrum, are to the actual peak determined by the Fourier spectrum. The pairwise comparison was carried out using the one-sided Wilcoxon criterion, thereby testing the hypothesis: the peaks identified by ARMA are located in median closer to those of the Fourier spectrum than the peaks found by Burg's method ($P_{i,\text{arma}}>P_{i,\text{burg}}$).

We have processed >590 spectra well approximated by the FITACF model. The resulting p-value when testing the one-sided hypothesis was $1.2\cdot10^{-7}$ (with the two-sided hypothesis giving $2.4\cdot10^{-7}$). This suggests that ARMA spectral peaks are indeed closer in position to the real peaks in the Fourier spectrum than those of Burg spectra. This is also confirmed by qualitative considerations — Burg spectra correspond to the simpler ARMA (8, 0) model, which has 2.5 times fewer regression parameters, being simpler than the ARMA (10, 10) model we employ [Cadzow, 1982].

Estimation of spectral mode width

For the final implementation of the method, it is necessary to determine not only the Doppler velocity, but also the amplitude and spectral width of each mode — all three main parameters obtained by the FITACF algorithm. Preliminary analysis has shown that parametric ARMA spectra for correlation functions are satisfactorily approximated by the Gaussian mixture (GM). The Gaussian function is defined by three parameters: amplitude (spectral power), mean (Doppler velocity) and standard (half spectral width) deviations. Thus, the parametric spectrum model $S(V)$ has the form

$$S(V) = \sum_{i=1}^{N} \frac{2A_i}{\sqrt{2\pi}W_{0i}} e^{-2\left(\frac{V-V_{0i}}{W_{0i}}\right)^2}. \quad (4)$$

Here, A_i, V_{0i}, W_{0i} are amplitude, velocity, and spectral width (in units of velocity); N is the number of signal spectral modes. It is apparent that the amplitude A_i of each parametric spectrum component has the meaning of the total power of this component (integral spectral power), and the multiplier for it is the corresponding normalization.

Thus, the procedure for finding parameters of parametric spectra is reduced to their fitting by GM $S(V)$ of a given number N, determined at the stage of searching for the number of peaks. The problem of finding these parameters is known and solved by optimization methods, such as the standard deviation of the parametric spectrum from its model. After fitting, the peaks are ordered by their energy ($A_i \geq A_{i+1}$) during data analysis. It is assumed here that the first modes generally correspond to informative signals; the last, to noise ones.

In what follows, we use the ARMA model for the full correlation function with linear approximation of the zero point, since it gives narrower spectral lines effective for further mode separation, and is also satisfactorily approximated by the sum of Gaussian functions.

We called the algorithm Arma Analysis of Multi-Peak ACF (AAMPACF).

FEATURES OF THE MODE STRUCTURE DURING THE PERIOD MAY 29 – JUNE 02, 2025

Multi-mode signals are the events that are regularly observed [Schiffler et al., 1997; Huber and Sofko, 2000; Danskin et al., 2004; Shepherd et al., 2003; Koustov et al., 2005] and easily determined from the parametric spectral estimate by the ARMA model, which gives three parameters for each mode: integral power, spectral shift, and spectral width. Let us look at the properties of signals with different numbers of modes, using EKB and MAGW radar observations of the geomagnetic storm on May 29 – June 02, 2025 as an example. The choice of the period is related to high velocities of irregularities observed during geomagnetic disturbances. This allows us to test the method's efficiency over a wide range of velocities, spectral widths, and geophysical conditions and to compare the results with the FITACF algorithm as in [Danskin et al., 2004], yet for the full number of spectral lines, not just for two.

Estimation of the maximum number of signal modes

It is important for a researcher to interpret signal spectral peaks. It is known that a signal contains noise of various nature and the so-called bad lags of the correlation function, where the signal is absent due to sounding signal characteristics [Ribeiro et al., 2013]. While the algorithm seems to be relatively resistant to the presence of bad lags, associated with characteristics of sounding signals in which the correlation function cannot be measured and is often equated to zero (see Figure 1), the noise level causes its own distortions in the number and characteristics of signal spectral peaks. We can therefore expect that some of the spectral peaks may be related to noise, and we need to estimate the number of peaks that can be considered actual signals. Let us use two methods for statistically estimating this number: from distribution of Doppler velocities of different modes and from the amplitude of different modes. In both cases, we can assume that the modes of the highest order (the last, least energetic) will be the least significant (noise).

Figure 2 illustrates the distribution of Doppler velocities of various signal modes observed by the EKB and MAGW radars during the period May 29 – June 02, 2025.

It can be assumed (see Figure 2) that there are no more than eight modes in the signal; at higher modes, the distribution of mode velocities becomes similar to the uniform (noise) one.

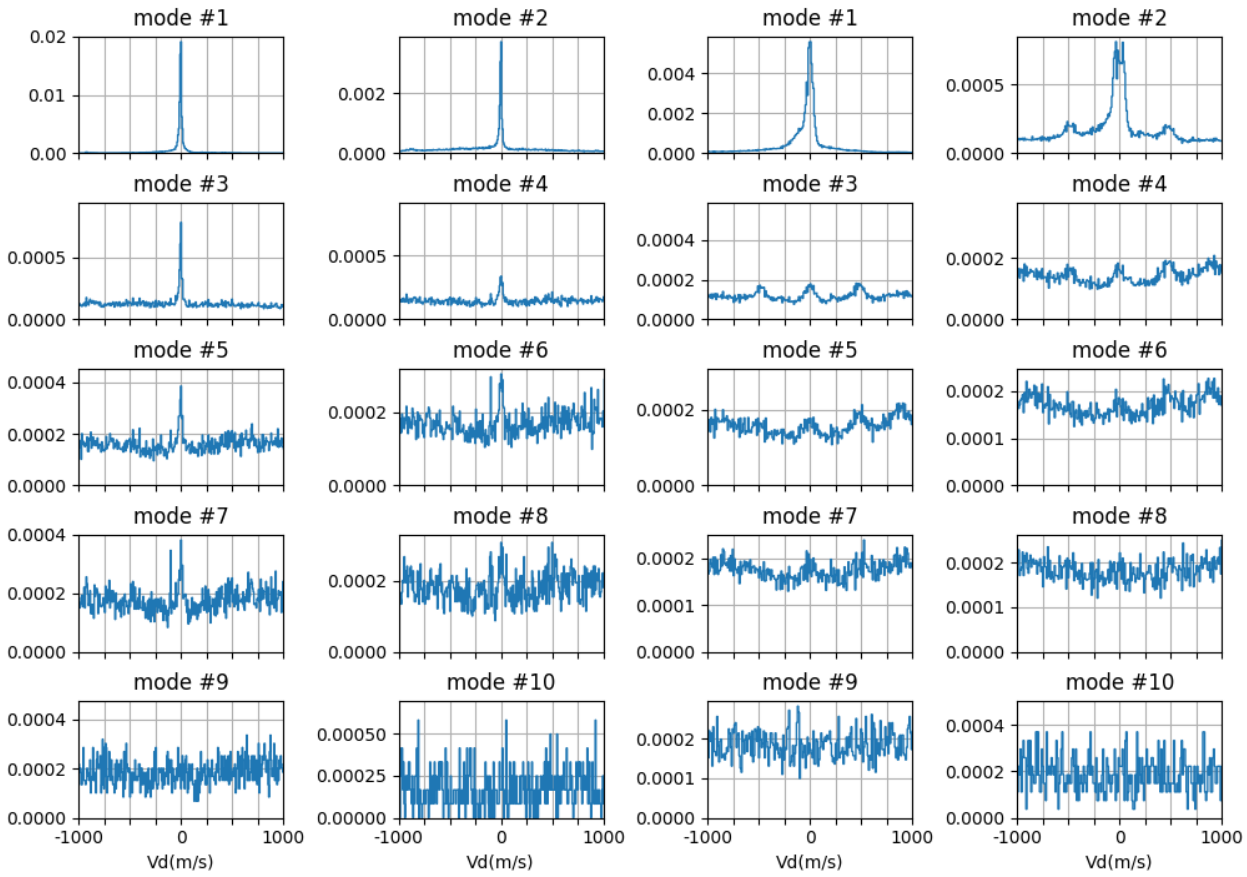

Figure 2. Distribution of Doppler velocities of AAMPACF modes observed in the EKB (left) and MAGW (right) radars for May 29 – June 02, 2025

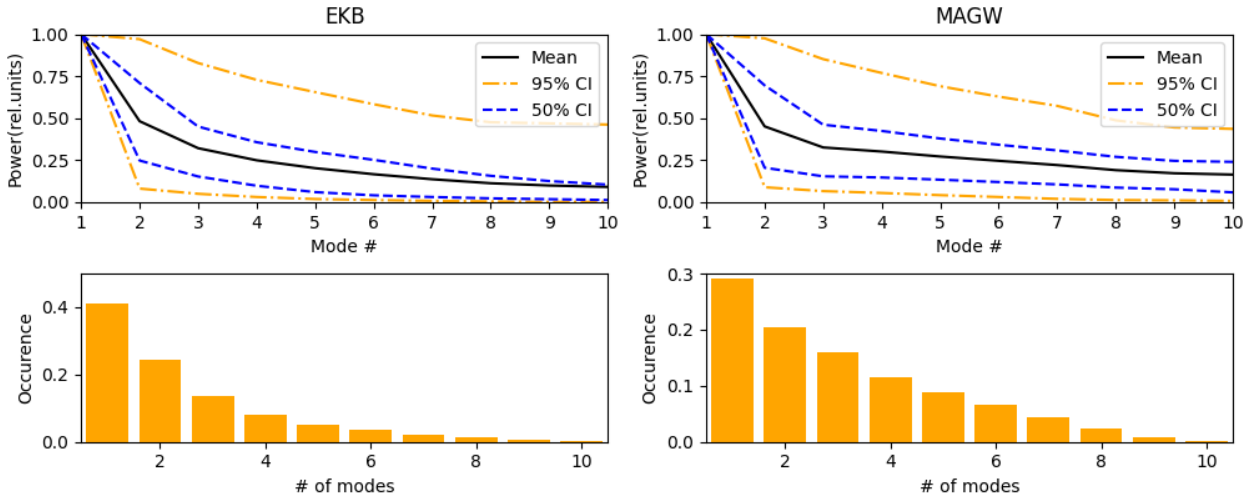

Figure 3. Relative ratio between peak amplitudes for different radars (top). Average value (solid line); confidence intervals of 50 % (dashed lines) and 95 % (dash-dot lines). At the bottom is the distribution of the number of peaks with amplitudes above 0.01 for the EKB (left) and MAGW (right) radars. Data for May 29 – June 02, 2025

Figure 3, *a*, *b* depicts the distribution of amplitudes of various signal modes observed by the EKB and MAGW radars relative to the mode with a maximum amplitude. 50 % and 95 % confidence intervals of observation for each order mode in the signal are given. The interval method shows that for the 50 % confidence interval the number of modes ranges from 1 (MAGW) to 3 (EKB); and for the 95 % interval, 1. The threshold amplitude separating noise signals from non-noise ones can therefore be considered to be ~0.5 of the maximum peak corresponding to the upper limit of the 95 % confidence interval for the 10th noise mode. Thus, although we cut off many significant modes in the signal, we do not miss most of the noise modes.

Figure 3, *c*, *d* illustrates the distribution of observed signals by the number of modes in them. From Figure 3 we notice that single-mode signals predominate in both radars, with the number of single-mode signals in the

EKB radar being ~40 %; and in the MAGW radar, ~30 %. Note that the analysis deals with the geomagnetically disturbed period May 29 – June 02, 2025; under quiet conditions, probabilities of observing a different number of modes may vary. According to [Danskin et al., 2004], two-mode spectra were recorded by the Hankasalmi SuperDARN radar with Burg's method in 35 % of cases, which suggests that there were ~65 % of single-mode signals. This indicates that our results are in reasonable agreement with previous observations.

Comparing AAMPACF and FITACF results

It is important to compare the results obtained by the FITACF and AAMPACF algorithms. It is obvious that for most cases the Doppler velocities obtained by the new method should be close to the results obtained by FITACF, which has been tested many times [Koustov et al., 1997, 2009, 2019; Xu et al., 2008; Bahcivan et al., 2013; Koustov et al., 2020; Ponomarenko et al., 2025]. It is also evident that in the case of single-mode signals (when we observe only one powerful peak in the spectrum and by power is meant not the intensity of the spectral component, but its integral intensity over frequency), which fit the FITACF model, we should obtain the best match. For checking purposes, the two methods have been applied to the MAGW and EKB radar data for May 29 – June 02, 2025 (Figures 4, 5).

Figure 4, *a*, *b* comparatively analyzes velocities of only single-mode signals — the dependence of Doppler velocities determined by the AAMPACF and FITACF algorithms. The velocities are seen to be determined by both algorithms almost similarly. The RMS error increases with decreasing velocity and is ~88 m/s for the EKB radar and 56 m/s for the MAGW radar.

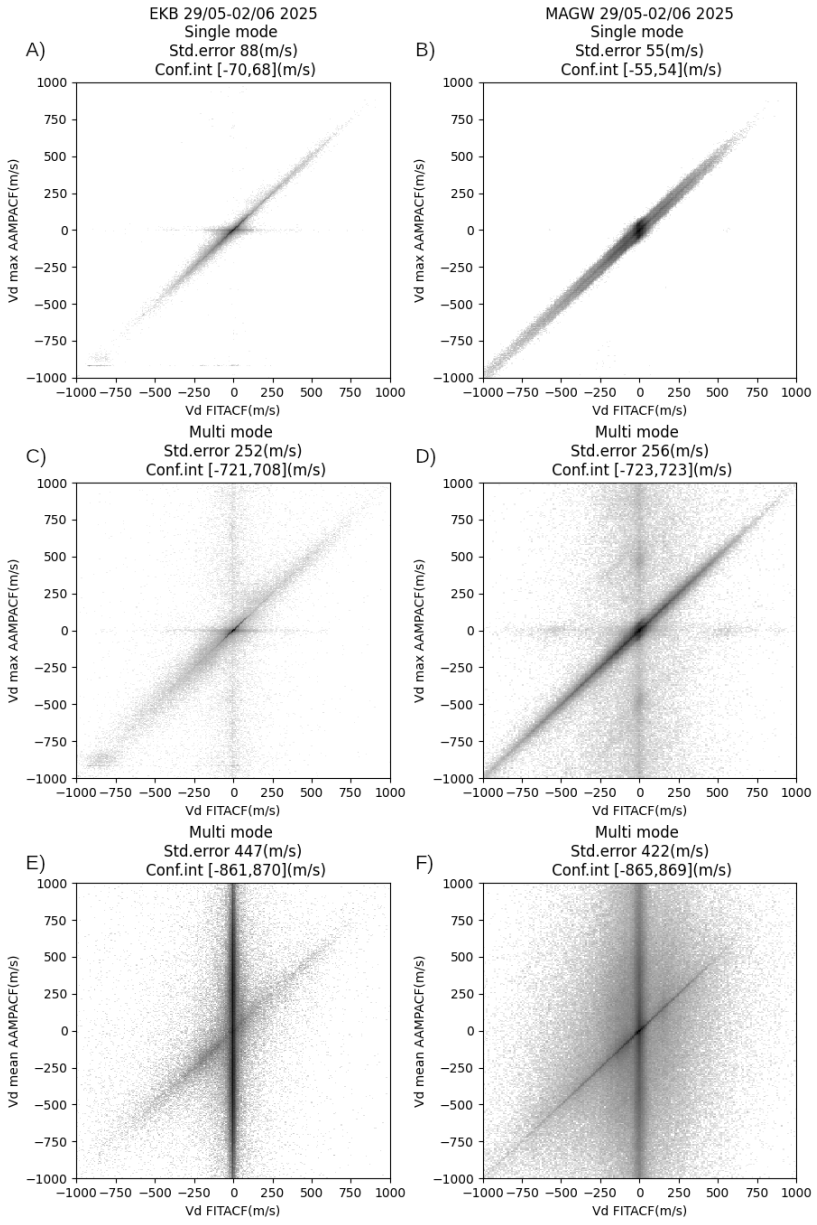

Figure 4. Comparison between velocities obtained by the AAMPACF and FITACF algorithms on May 29 – June 02, 2025: single-mode signals (*a*, *b*); multi-mode signals (*c*, *d*) in the component with maximum amplitude; average velocities (*e*, *f*) over the entire spectrum with a weight equal to the spectral amplitude of the mode $A_i W_0$

Panels *c*, *d* comparatively analyze Doppler velocities measured by both algorithms for multi-mode signals, with the parameters estimated for the maximum signal mode:

$$V_{\max} = V_{0j} : j = \arg\max\left(A_i\right), \\ W_{\max} = W_{0j} : j = \arg\max\left(A_i\right). \quad (5)$$

Panels *e*, *f* perform a comparative analysis of Doppler velocities obtained by both algorithms for all signals, with the parameters estimated by averaging over modes:

$$V_{\text{mean}} = \sum A_i W_{0i} V_{0i} \Big/ \sum A_i W_{0i}, \\ W_{\text{mean}} = \sqrt{\sum A_i W_{0i} \left(\left(V_{0i} - V_{\max}\right)^2 + W_{0i}^2\right) \Big/ \sum A_i W_{0i}}. \quad (6)$$

It can be seen (*c*–*f*) that, although there are a certain number of cases in which the velocities are similar, it is smaller than that for single-mode signals. The main problems arise for signals that the FITACF algorithm defines as low-velocity, but they in fact consist of several modes.

In Figure 5, *a*, *b* are dependences of spectral widths determined by the AAMPACF and FITACF algorithms. There are some similarities in the spectral widths, especially for the MAGW radar, but their relative differences are much larger than those between estimated velocities.

Panels *c*, *d* and *e*, *f* show spectral widths for the case of searching for the width of the maximum mode and the average spectral width respectively. It is evident that the spectral widths of FITACF and AAMPACF cannot be considered sufficiently similar.

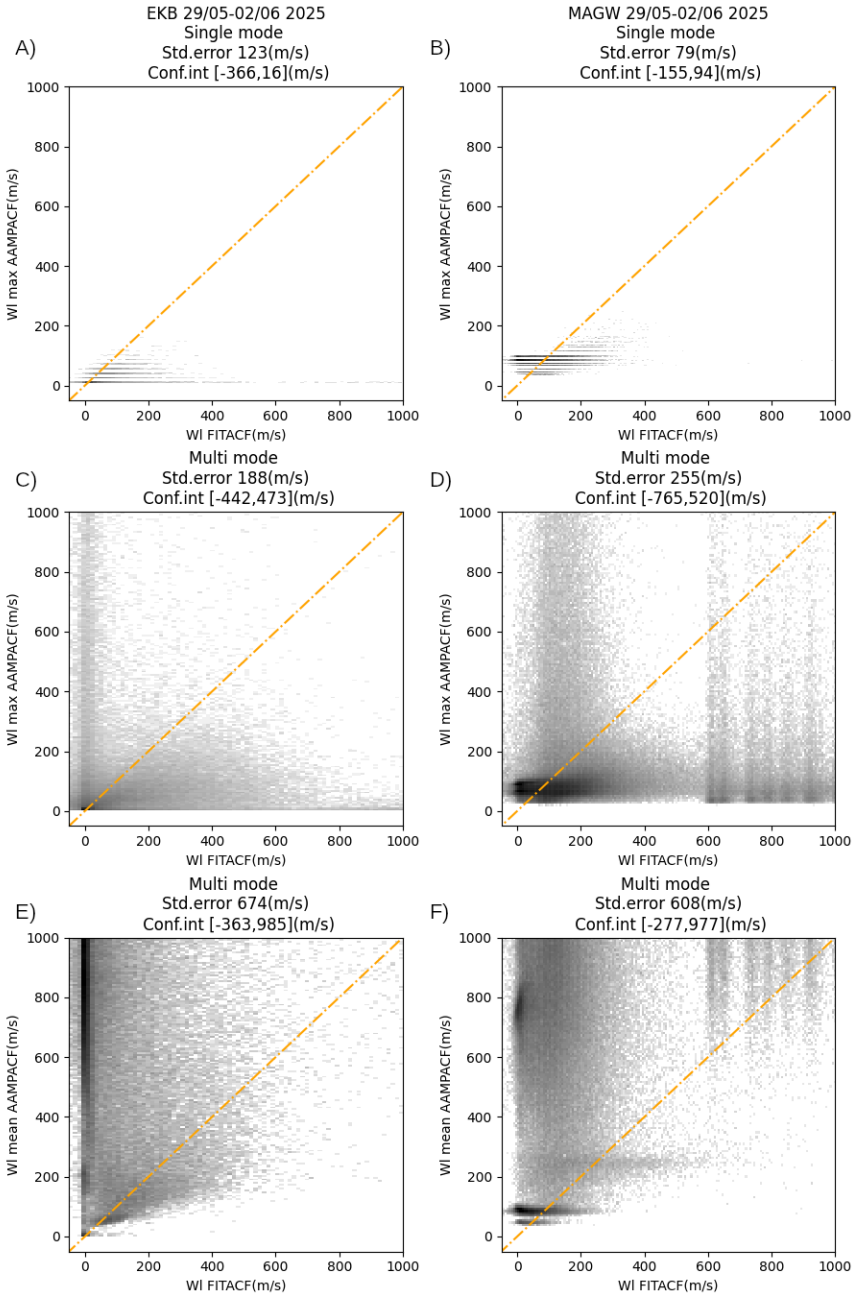

Figure 5. The same as in Figure 4 for spectral widths

Thus, the FITACF data agrees well with the AAMPACF data in terms of velocity for single-mode spectra; and fairly well, in terms of spectral width. In the case of multi-mode spectra, the results vary significantly. We can conclude that FITACF should be applied only to single-mode signals, and multi-mode signals should be analyzed separately.

It is clear from Figures that FITACF most closely evaluates the maximum mode in the spectrum, estimating not the entire signal spectrum, but only its most powerful mode. Therefore, the closest fit between AAMPACF and FITACF is apparently achieved by searching for the mode with the maximum integral amplitude and determining its characteristics: velocity and spectral width.

Note that such a high correlation when comparing velocities was not observed in [Danskin et al., 2004]. This may be due to the fact that the main focus was on analyzing low-speed events. We observe an effect similar to that described in [Danskin et al., 2004] in the region of low velocities (when the FITACF velocities are almost zero, although the parametric spectrum gives higher velocities) (see Figure 4) in AAMPACF data; it is especially pronounced for the MAGW radar (the case of single-mode signals).

The obvious disadvantage of the AAMPACF method is its computational resource intensity, especially at the stage of determining amplitudes and spectral widths, which also hinders its practical application.

Description of the AAMPACF algorithm

Thus, the final AAMPACF algorithm consists of the following steps.

1. Completion of the left part of the received signal correlation function with complex conjugate; linear approximation of the zero delay in amplitude and phase.

2. Processing of the obtained correlation function by the ARMA algorithm with regression length of 10 in AR and 10 in MA.

3. Construction of a parametric spectrum from the obtained regression coefficients, determination of the position of V_{0i} of local maximum values in it with >0.1 amplitude of the amplitude of the maximum peak.

4. Construction of Gaussian mixture model (4) for the obtained parametric spectrum, determination of integral amplitudes A_i and spectral widths W_{0i} of these modes by the least square method.

5. Sorting of the obtained values in descending order of the integral amplitude A_i to leave only peaks with $A_i/A_0>0.5$.

When comparing with FITACF, peaks with very high velocities $|V_{0i}|>1000$ m/s are excluded and only mode parameters with the maximum integral amplitude A_i are used.

DISCUSSION

Figures 6, 7 illustrate spatiotemporal features of the mode composition observed by the EKB and MAGW radars. There is the previously observed continuity (see Figures 6, 7, *a–f* representing only single-mode signals) between the characteristics determined by AAMPACF and FITACF for single-mode signals.

Figures 6, 7, *g–n* displaying only multi-mode signals indicate (in particular according to MAGW radar data) that multi-modal regions can cover large spatial areas. This may be due, for example, to the fact that in the presence of high spatial gradients of parameters several signals of various types can be observed in the region covered by a single sounding pulse (~45 km long) [Schiffler et al., 1997]. The EKB radar also records small spatially localized multi-modal regions usually associated with ionospheric scattering (the region of 21 UT in Figure 6, *g–n*). Thus, the observed multi-mode spectra are regular and can occupy large space-time regions, which is in line with earlier results obtained by Burg's method [Schiffler et al., 1997; Huber, Sofko, 2000; Danskin et al., 2004].

The analysis presented in the paper has shown that FITACF and AAMPACF in the case of single-mode signals give very similar Doppler velocities, but significantly different spectral widths. FITACF and AAMPACF in the case of multi-mode signals are difficult to compare. A good comparison is obtained if parameters of only the most powerful spectral mode are compared with FITACF.

This suggests that in most cases the FITACF algorithm evaluates a multi-mode signal as a single-mode with a changed spectral width, and in the AAMPACF algorithm these modes can be separated. In the cases where qualitative analysis is required or single-mode signals are observed, we can apply the FITACF algorithm. For a more detailed analysis, in particular in the case of multi-mode signals, it is worthwhile employing AAMPACF. Another advantage of AAMPACF is the positivity of all spectral widths it identifies, regardless of signal complexity.

From a physical point of view, the multi-mode signal analysis can be used in three cases. The first case (for example, when examining the cusp [Schiffler et al., 1997]) is when there are regions with different Doppler velocities inside the analyzed volume (~45 km in range), which makes it possible to study convection with higher spatial resolution exceeding the spatial resolution of an individual pulse [Huber, Sofko, 2000]. The second case [Danskin et al., 2004] is the analysis of spectra composed of instabilities of two types: for example, Farley—Buneman and gradient-drift. The third case is the simultaneous observation of several signal modes propagating along different paths, but arriving with the same delay.

Obviously, to interpret multi-mode signals, it is necessary to use classification methods that are resistant to spectral width changes. It is impossible to apply the standard algorithm of classifying signals as ionospheric and scattered from Earth's surface [Ponomarenko et al., 2007] to this problem, since the spectral widths identified by the two methods differ significantly. One of the potential methods of such classification may be the algorithm [Berngardt, Lavygin, 2026] based on ray tracing, which requires accurate measurements of the elevation angle of arrival of signals and weakly depends on spectral width.

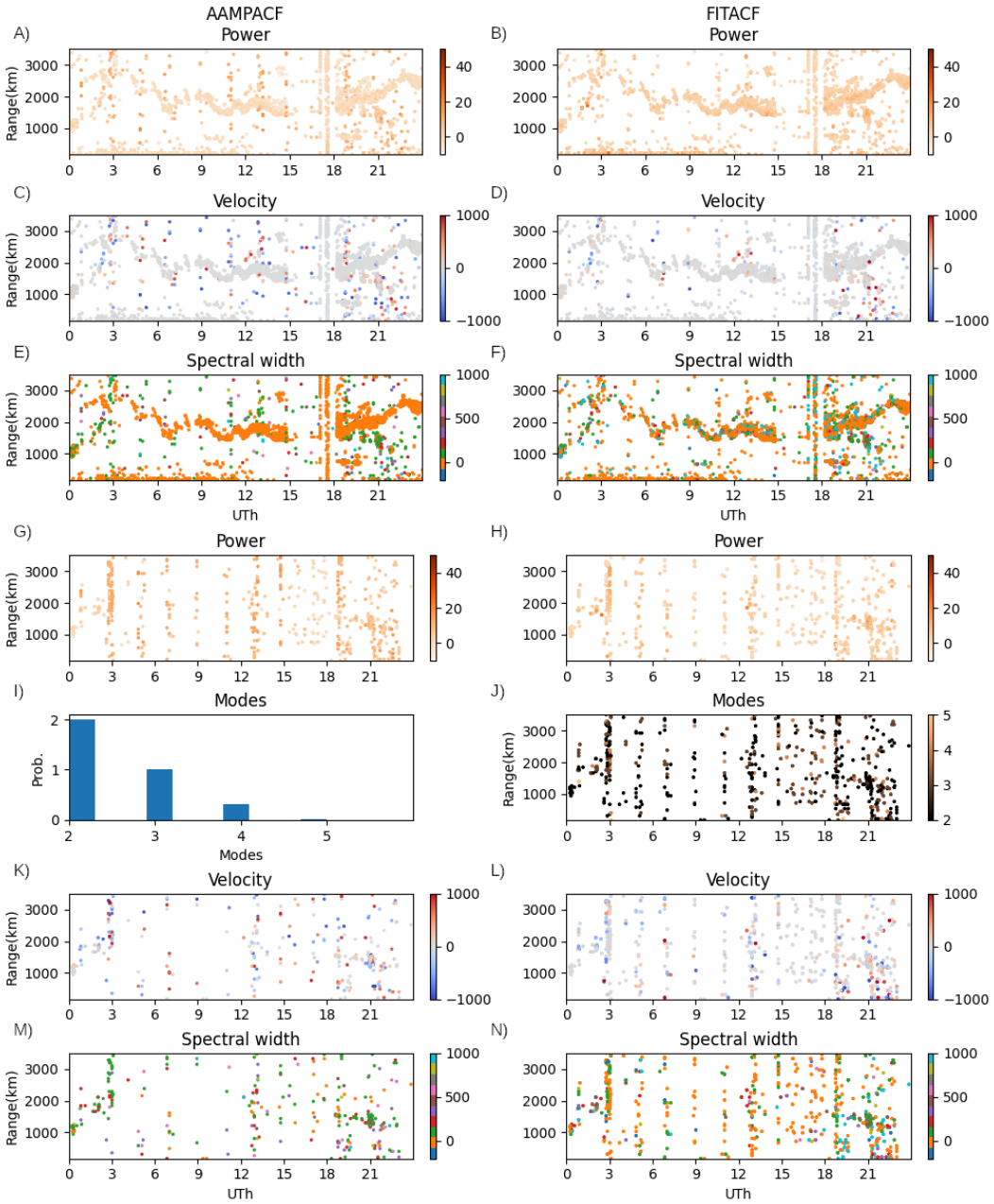

Figure 6. Parameters of single-mode signals on May 31, 2025 for the EKB radar (11 MHz frequencies), beam 3, channel 1: *a–f* — single-mode signals; *g–n* — multi-mode signals. On the left are the parameters obtained by AAMPACF; on the right, by FITACF

A possible interpretation of the class numbers, used below, from a physical point of view is given in [Berngardt, Lavygin, 2026]. Assuming that all signal modes come from the same elevation angle, we can obtain the error matrix shown in Figure 8.

It can be seen that most of the modes are determined in a similar way from FITACF and AAMPACF data, which is due to the adequate calculation of velocities by both algorithms in the single-mode case and with a relatively small number of multi-mode signals. The main differences in AAMPACF fall within poorly defined classes No. 6 (too high velocities or spectral widths) and No. 37 (different versions of the classifier identify the class variously). The appearance of class No. 6 is easily explained: there are high-frequency modes in spectra, and after they are identified by the AAMPACF algorithm, they are assigned to class No. 6 and ignored by the FITACF algorithm. The appearance of class No. 37 is probably due to complex scattering patterns that were not previously taken into account when training the classifier (the classifier was trained on FITACF data from SuperDARN and SECIRA radars). They are, therefore, classified uncertainly and assigned by the algorithm to class No. 37.

Figure 9, *a* illustrates the mode distribution of signals processed by the AAMPACF and FITACF algorithms. The fundamental new observations are seen to correspond to classes No. 6 (poorly interpreted class) and No. 37 (vaguely interpreted class) within the classifier [Berngardt, Lavygin, 2026]. The per-

centage of new signals for the remaining classes is ~5–10 %.

Panel *b* shows the distribution of signals that are interpreted after AAMPACF differently than after FITACF. It is apparent that signals interpreted after FITACF as class No. 6 (poorly interpreted class) can be interpreted differently in 20 % of cases after AAMPACF. The leaders in possible different interpretation are also classes Nos. 26, 28, 32, and 37 (all are uncertainly defined classes within the classifier [Berngardt and Lavygin, 2026]), which indicates a significant proportion of poorly classified signals that can be interpreted differently when processed by the AAMPACF algorithm.

The statistics in Figure 9, *c* confirm this trend: the use of AAMPACF generally increases the number of detected signals attributed to different scattering types (due to the fact that it can detect several signal modes), and considerably increases the number of signals in poorly defined classes, in particular in classes Nos. 6, 26, 28, 31, 32, and 37, presumably introducing noise signals into them. The number of signals when AAMPACF data is classified decreases only in class 32 (see Figure 9, *a*), characterized by too high scattering heights [Berngardt, Lavygin, 2026]. Some of these signals are interpreted differently, mainly as having too high velocities (class No. 6).

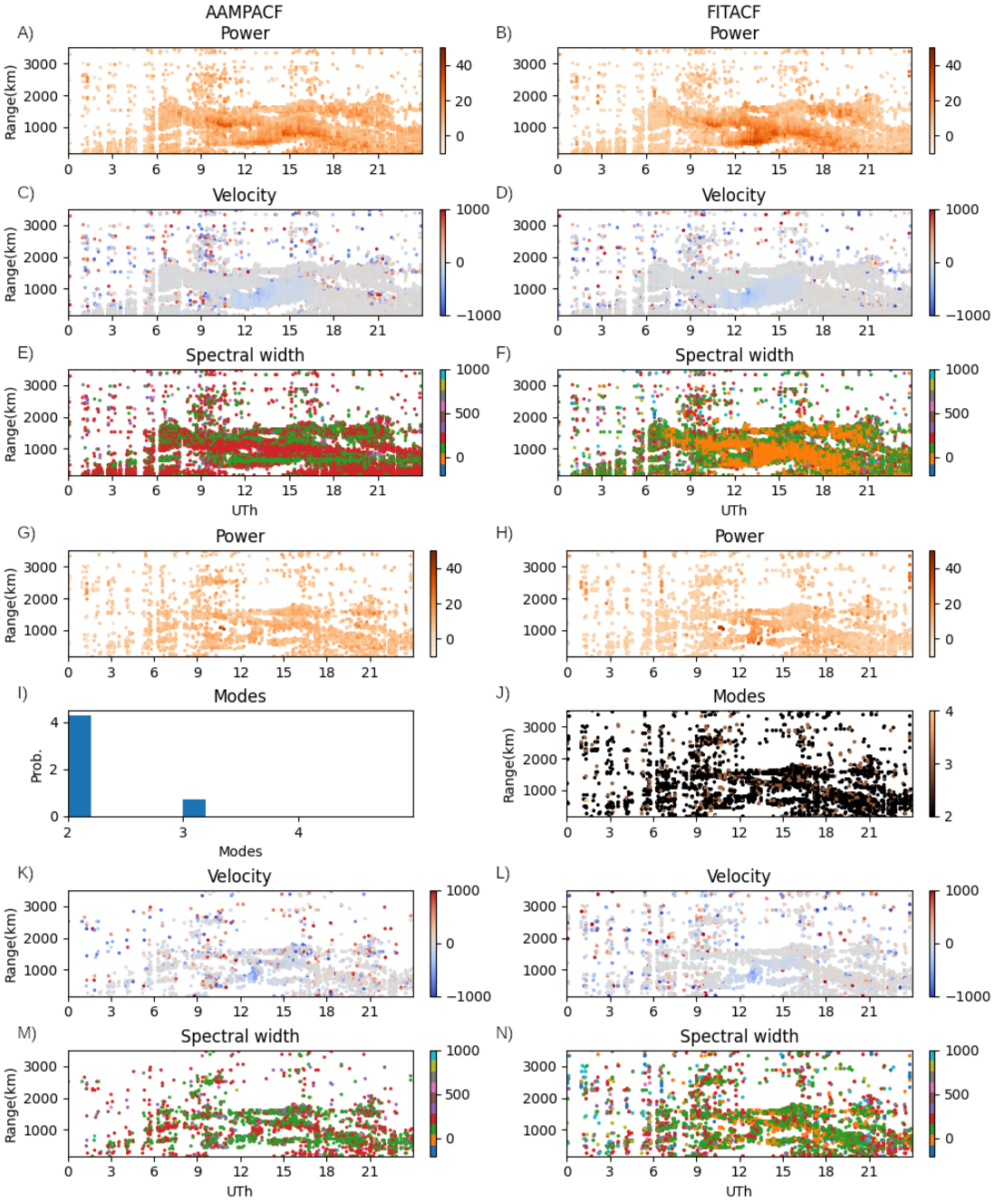

Figure 7. Parameters of multi-mode signals on May 31, 2025 for the MAGW radar (8 MHz frequencies), beam 3, channel 1: *a–f* — single-mode signals; *g–n* — multi-mode signals. On the left are parameters received by AAMPACF; on the right, by FITACF

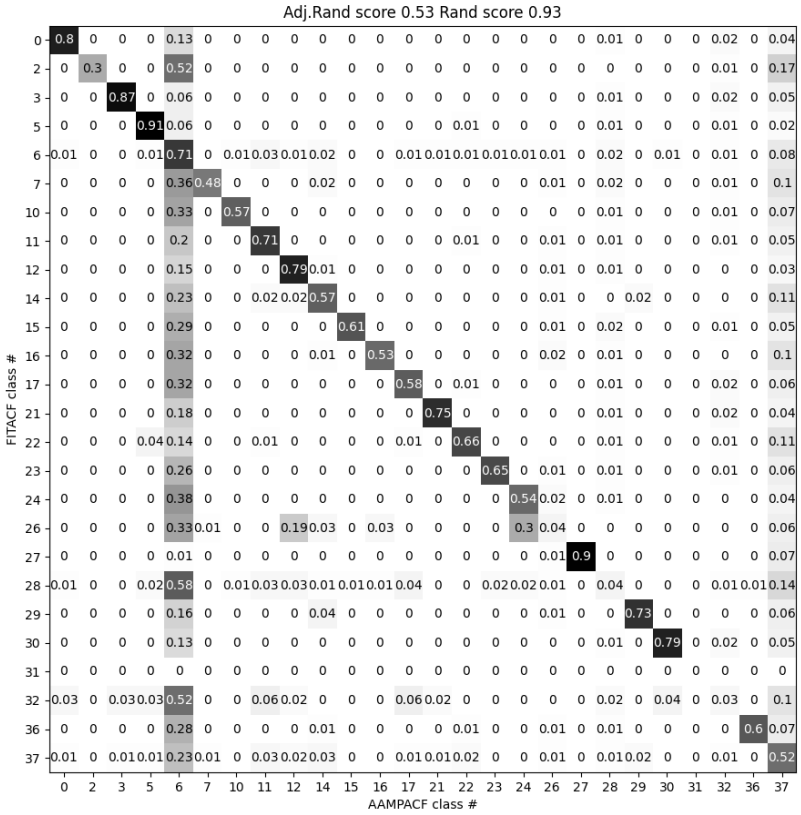

Figure 8. Error matrix for classifying signals processed by the FITACF and AAMPACF algorithms on May 29 – June 02, 2025. The diagonal corresponds to an identical classification of the same signal (its mode) processed by the two algorithms

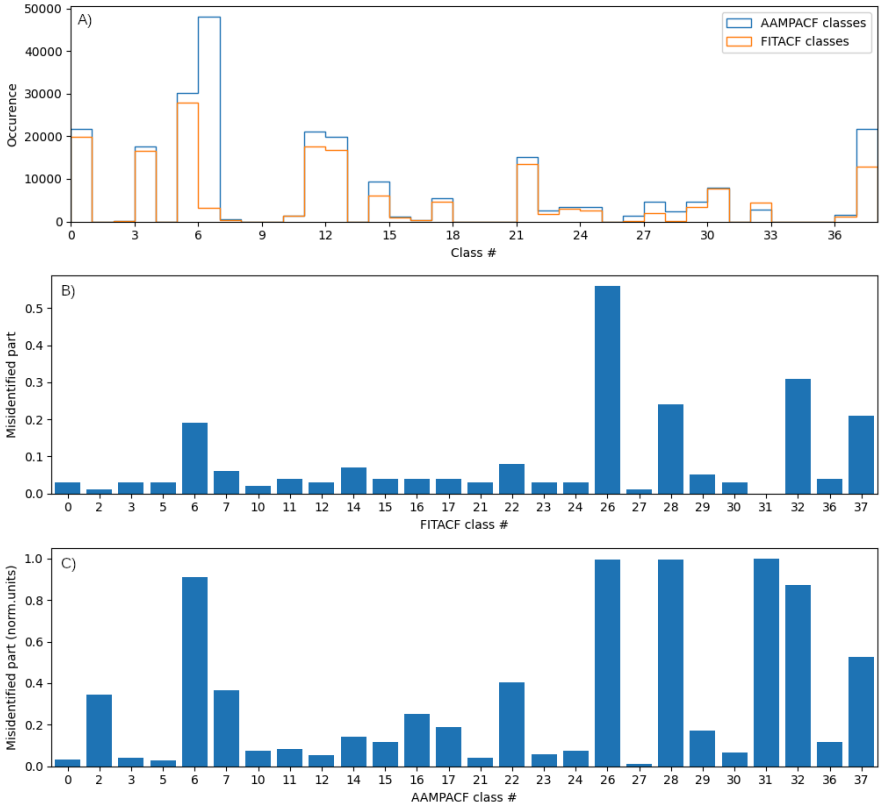

Figure 9. Proportion of signals of various types (*a*) when classified by FITACF and AAMPACF [Berngardt, Lavygin, 2026]; *b* — proportion of signals classified after AAMPACF differently than after FITACF; *c* — proportion of signals that are classified after FITACF differently than after AAMPACF

CONCLUSION

The paper presents the algorithm for estimating parameters of coherent scattering signals AAMPACF (Arma Analysis of Multi Peak ACFs), based on parametric estimation of their spectra by the ARMA model, followed by fitting the obtained spectra with the sum of Gaussian functions. Each spectrum is described by amplitude, Doppler velocity, and spectral width. The algorithm is a development of the method proposed in [Schiffler et al., 1997], and differs in the use of the more complex regression model ARMA, consideration of correlation function features, and determination of three parameters for each peak (mode) found: amplitude, velocity, and spectral width.

The analysis presented in the paper has shown that FITACF and AAMPACF for single-mode signals give very similar Doppler velocities; FITACF often yields different spectral widths as compared to AAMPACF, although on average they are somewhat similar.

FITACF and AAMPACF in the case of multi-mode signals are difficult to compare, and the result depends on the method used for processing AAMPACF peaks. The comparison has revealed that the best continuity between the parameters with FITACF is provided by the analysis of the mode with maximum integral spectral power. This allows us to analyze and interpret each mode as a physically explicable scattering, as well as to utilize the AAMPACF algorithm as an effective replacement for the FITACF algorithm.

The multi-mode AAMPACF analysis increases the number of detectable signals of various types and can be used to expand the diagnostic capabilities of the SECIRA/SuperDARN radars.

The advantages of the model include the physical correctness of each mode: by definition, each mode has positive spectral widths and a fairly exact fit between Doppler velocities and well-verified FITACF results in the case of single-mode signals.

The disadvantages of the model are its computational resource intensity, in particular when determining mode amplitude and spectral width, although today's computers in view of simplicity of parallelizing the task can process data from SECIRA/SuperDARN radars in real time.

The program is implemented in C and Python for parallel processing of an ACF signal, presented in the RAWACF file format standard for SECIRA/SuperDARN radars, and saves the results in CBOR format — one of the modern resource-efficient and self-describing formats for exchanging typed data. The RSTLite library is used to work with radar files [https://github.com/vtsuperdarn/RSTLite]. Currently, the program on the computer with a 32-thread processor, a clock frequency of 2.2 GHz, and 16 GB RAM processes 8 days of data with original autocorrelation functions per day.

The program code is available at [https://github.com/berng/AAMPACF].

The results were obtained using the Core Shared Research Facility "Angara" of ISTP SB RAS [https://ckp-rf.ru/catalog/ckp/3056/]. The work was financially supported by the Ministry of Science and Higher Education in terms of maintaining the EKB and MAGW radars and by RSF in terms of research (grant No. 24-22-00436) [https://rscf.ru/project/24-22-00436/].

REFERENCES

Bahcivan H., Nicolls M.J., Perry G. Comparison of SuperDARN irregularity drift measurements and F-region ion velocities from the resolute bay ISR. *J. Atmos. Solar-Terr. Phys*. 2013, vol. 105-106, pp. 325–331. https://doi.org/10.1016/j.jastp.2013.02.002.

Barthes L., André R., Cerisier J.-C., Villain J.-P. Separation of multiple echoes using a high-resolution spectral analysis for SuperDARN HF radars. *Radio Sci*. 1998, vol. 33, iss. 4, pp. 1005–1017. https://doi.org/10.1029/98RS00714.

Berngardt O., Lavygin I. Self-learning signal classifier for HF coherent scatter radars. *Adv. Space Res.* 2026, vol. 77, iss. 3, pp. 3527–3548. https://doi.org/10.1016/j.asr.2025.11.074.

Berngardt O.I., Grkovich K.V., Fedorov R.R. Synthesis of symmetric sounding sequences for Ekaterinburg coherent decameter radar. *Radiophysics and Quantum Electronics*, 2020, vol. 62, iss. 11, pp. 721–733. https://doi.org/10.1007/s11141-020-10018-y.

Berngardt O.I., Kusonsky O.A., Poddelsky A.I., Oinats A.V. Self-trained artificial neural network for physical classification of ionospheric radar data. *Adv. Space Res.* 2022, vol. 70, iss. 10, pp. 2905–2919. https://doi.org/10.1016/j.asr.2022.07.054.

Cadzow J.A. Spectral estimation: An overdetermined rational model equation approach. *Proc. IEEE*. 1982, vol. 70, iss. 9, pp. 907–939. https://doi.org/10.1109/PROC.1982.12424.

Chisham G., Lester M., Milan S.E., et al. A decade of the Super Dual Auroral Radar Network (SuperDARN): scientific achievements, new techniques and future directions. *Surv. Geophys*. 2007, iss. 28, pp. 33–109. https://doi.org/10.1007/s10712-007-9017-8.

Danskin D.W., Koustov A.V., Makarevitch R.A., Lester M. Observations of double-peaked E region coherent spectra with the CUTLASS Finland HF radar. *Radio Sci*. 2004, vol. 39, iss. 2, p. RS2006, https://doi.org/10.1029/2003RS002932.

Greenwald R.A., Baker K.B., Dudeney J.R., et al. DARN/SuperDARN: A global view of the dynamics of high-latitude convection. *Space Sci. Rev.* 1995, vol. 71, pp. 761–796. https://doi.org/10.1007/BF00751350.

Huber M., Sofko G.J. Small-scale vortices in the high-latitude F region. *J. Geophys. Res.: Space Phys.* 2000, vol. 105, iss. A9, pp. 20885–20897. https://doi.org/10.1029/1999JA000417.

Koustov A.V., Koehler J.A., Sofko G.J. et al. Relationship of the SAPPHIRE-North merged velocity and the plasma convection velocity derived from simultaneous SuperDARN radar measurements. *J. Geophysi. Res.: Space Phys*. 1997, vol. 102, iss. A2, pp. 2495–2501. https://doi.org/10.1029/96JA03351.

Koustov A.V., Danskin D.W., Makarevitch R.A., Gorin J.D. On the relationship between the velocity of E-region HF echoes and **E**×**B** plasma drift. *Ann. Geophys.* 2005, vol. 23, iss. 2, pp. 371–378. https://doi.org/10.5194/angeo-23-371-2005.

Koustov A.V., St.-Maurice J.-P., Sofko G.J., et al. Three-way validation of the Rankin Inlet PolarDARN radar velocity

measurements. *Radio Sci*. 2009, vol. 44, iss. 4. p.RS4003. https://doi.org/10.1029/2008RS004045.

Koustov A.V., Lavoie D.B., Kouznetsov A.F., et al. A comparison of cross-track ion drift measured by the Swarm satellites and plasma convection velocity measured by SuperDARN. *J. Geophys. Res.: Space Phys*. 2019, vol. 124, iss. 6, pp. 4710–4724. https://doi.org/10.1029/2018JA026245.

Koustov A.V., Luciuk M.R., Gillies R.G., et al. Velocity of SuperDARN echoes at intermediate radar ranges. *Radio Sci*. 2020, vol. 55, iss. 11. p. e2020RS007142.

Nguyen T.T., Devlin J.C., Elton D.M., et al. A comparison of FFT-based techniques for Doppler velocity estimation in SuperDARN radars. In: *2014 International Symposium on Information Theory and its Applications*, pp. 75–79.

Nishitani N., Ruohoniemi J.M., Lester M., et al. Review of the accomplishments of mid-latitude Super Dual Auroral Radar Network (SuperDARN) HF radars. *Progress in Earth and Planetary Science*. 2019, vol. 6, iss. 1. https://doi.org/10.1186/s40645-019-0270-5.

Ponomarenko P.V., Waters C.L., Menk F.W. Factors determining spectral width of HF echoes from high latitudes. *Ann. Geophys*. 2007, vol. 25, iss. 3, pp. 675–687. https://doi.org/10.5194/angeo-25-675-2007.

Ponomarenko P., Ghalamkarian Nejad M., Koustov A.V. Application of SuperDARN interferometry for improved estimates of Doppler velocity and echo geolocation. *Radio Sci*. 2025, vol. 60, iss. 1, p. e2024RS008084. https://doi.org/10.1029/2024RS008084.

Ribeiro A.J., Ruohoniemi J.M., Ponomarenko P.V., et al. A comparison of SuperDARN ACF fitting methods. *Radio Sci*. 2013, vol. 48, iss. 3, pp. 274–282. https://doi.org/10.1002/rds.20031.

Schiffler A., Sofko G., Newell P.T., Greenwald R. Mapping the outer LLBL with SuperDARN double-peaked spectra. *Geophys. Res. Lett*. 1997, vol. 24, iss. 24, pp. 3149–3152. https://doi.org/10.1029/97GL53304.

Shepherd S.G., Ruohoniemi J.M., Greenwald R.A. Direct measurements of the ionospheric convection variability near the cusp/throat. *Geophys. Res. Lett*. 2003, vol. 30, iss. 21, p. 2109. https://doi.org/10.1029/2003GL017668.

Xu L., Koustov A.V., Xu J.S., et al. A 2D comparison of ionospheric convection derived from SuperDARN and DMSP measurements. *Adv. Space Res*. 2008, vol. 42, iss. 7, pp. 1259–1266. https://doi.org/10.1016/j.asr.2007.06.044.

Zhang J., Lan A., Yan J., et al. Development of the Chinese Dual Auroral Radar Network and preliminary results. *Space Weather*. 2024, vol. 22, iss. 10. p. e2024SW004131. https://doi.org/10.1029/2024SW004131.

URL: https://github.com/vtsuperdarn/RSTLite (accessed December 12, 2025).

URL: https://github.com/berng/AAMPACF (accessed December 12, 2025).

URL: https://pgia.ru/data/spaceweather/ (accessed December 12, 2025).

URL: https://ckp-rf.ru/catalog/ckp/3056/ (accessed December 12, 2025).

Original Russian version: Berngardt O.I., published in Solnechno-zemnaya fizika. 2026, vol. 12, no. 2, pp. 84–96. https://doi.org/10.12737/szf-122202609.

How to cite this article

Berngardt O.I. Method for estimating parameters of multi-mode signals measured at SECIRA radars. *Sol.-Terr. Phys.*. 2026, vol. 12, iss. 2, pp. 76–88. https://doi.org/10.12737/stp-122202609.